Applied Catalysis B: Environmental 205 (2017) 404–411

Contents lists available at ScienceDirect

Applied Catalysis B: Environmental

journal homepage: www.elsevier.com/locate/apcatb

Synergistic effects of persistent free radicals and visible radiation on peroxymonosulfate activation by ferric citrate for the decomposition of organic contaminants

Lianshun Luo, Di Wu, Dejun Dai, Zhiyuan Yang, Likun Chen, Qinbo Liu, Junchu He, Yuyuan Yao*

National Engineering Lab of Textile Fiber Materials & Processing Technology (Zhejiang), Zhejiang Sci-Tech University, Hangzhou 310018, PR China

ARTICLE INFO

Article history:
Received 25 October 2016
Received in revised form
19 December 2016
Accepted 24 December 2016
Available online 26 December 2016

Keywords:
Persistent free radicals
Activated carbon fibers
Ferric citrate
Visible radiation
Reactive oxygen species

ABSTRACT

In this work, persistent free radicals (PFRs) of activated carbon fibers (ACFs) were innovatively coupled with Fe(III)–photocatalysts to construct a distinctive catalytic oxidation system, FeCit@ACFs/PMS/visible light. Herein, PFRs acted as an electron sink by donating electrons to ferric citrate (Cit-Fe), thereby accelerating the ligand-to-metal charge transfer (LMCT) processes that govern the rate-determining step of the reaction transforming Cit-Fe^{III} to Cit-Fe^{II}. Moreover, visible radiation can serve as another powerful assistor to further enhance the LMCT processes because Cit-Fe exhibits highly intrinsic photosensitivity. The synergistic enhancement effect of PFRs and visible light endowed the constructed FeCit@ACFs catalyst with strong catalytic activity, which could effectively activate peroxymonosulfate (PMS) to generate reactive oxygen species (ROS) for contaminants decomposition. To investigate the ROS generated in this experiment, we adopted a hybrid method that combines electron paramagnetic resonance technology with different radical scavengers, and the results indicated that $^{\bullet}OH$ and $SO_4^{\bullet-}$ were generated and played a major role in the catalytic oxidation process. This work provided a new insight into the positive role of PFRs and presented an up-to-date research domain of PFRs-enhanced catalysis. It also paved an avenue for developing high-efficiency processes for the generation of ROS, which can be subsequently used in environmental catalysis.

1. Introduction

Persistent free radicals (PFRs) have half-lives on the order of hours to days under various atmospheric conditions. They have been widely detected in combustion-generated particulate matters [1,2], sediments [3], and even in soils [4]. Owing to their persistence and radical reactivity, PFRs are attracting a lot of attention of researchers in biological and environmental fields. In previous research studies, it has been reported that PFRs are pernicious species, because they have the potential to induce oxidative stress that causes a variety of illnesses in exposed populations [5–7]. For example, Balakrishna et al. reported that neonates exposed to PFRs-containing combustion generated ultrafine particles developed significant pulmonary inflammation, and airway hyperreactivity; these ultrafine particles contain a significant number of PFRs [7]. Although reports have described how PFRs directly activate oxidants to oxidize organic compounds [8,9], very few studies have investigated the positive role of PFRs in various reactions.

It is worthwhile to mention that PFRs are also known as resonance-stabilized radicals, with an abundance of unpaired electrons. Therefore, PFRs can act as electron donors and bring about a sustainable electron transfer to other electron-acceptors, such as higher valent metals. In other words, PFRs reduce these metals by donating electrons [10,11]. Therefore, PFRs can accelerate some important catalytic redox processes, such as the iron-mediated catalytic cycle that activates oxidants used in the treatment of environmental contaminants; this cycle has an intrinsic drawback of slow reduction rate of iron. Thus, PFRs might play an important role in enhancing the catalytic oxidation performance of ROS (reactive oxygen species), which are used in the decomposition of contaminants. However, only a handful of research studies have reported about this positive effect of PFRs.

Over the past years, visible light-assisted catalysis has been recognized as an extremely promising technology for the treatment of organic pollutants [12–14]. In particular, ferric citrate (Cit-Fe) complexes have been thoroughly investigated (Reactions

* Corresponding author.
E-mail address: yyy0571@126.com (Y. Yao).

http://dx.doi.org/10.1016/j.apcatb.2016.12.060
0926-3373/

(1)–(4)) as they have low toxicity and high photoreactivity; it has been found that Cit-Fe complexes serve as outstanding photocatalysts [15,16]. However, previous research studies involving Cit-Fe catalysis mainly focused on the homogeneous media in which the reduction of Fe(III) ions underwent reduction through ligand-to-metal charge transfer (LMCT) processes (Reactions (1) and (2)): this is the key step to improving catalysis efficiency; these processes are sensitive to reaction conditions (especially pH) and it is easy to strictly control them [17]. In homogeneous media, Cit-Fe complexes have high mobility, so they may adversely affect the ecosystem. One of the most effective yet simple strategies is to develop the heterogeneous catalysts that can alleviate these limitations and enable the reuse of Cit-Fe catalyst. Recently, various supports, such as Nafion, zeolite, resin, and clay, have been used to develop the heterogeneous catalysts [18–21]. Compared to these supports, activated carbon fibers (ACFs) may be a more satisfactory candidate as it has remarkable characteristics. Firstly, ACFs is a kind of carbon material with highly microporous structure and remarkably high adsorption ability. Moreover, ACFs have a uniform micropore size distribution and a large surface area [22]. ACFs can be used to synthesize felts or fabrics of various types, while granular or powder supports cannot be used for the same. Thus, ACFs have more applications as compared to conventional supports that exist in either granular or powdered form. Most importantly, ACFs was the ideal representative of PFRs, and PFRs in ACFs are capable of providing electrons to Cit-Fe, which might contribute to further accelerating the LMCT processes and bring about the reduction of Fe(III) to Fe(II) state. And our previous reports have demonstrated that PFRs in ACFs initiate electron transfer and improve the catalytic activity of iron porphyrin (hemin), which is used to activate H_2O_2 and bring about the degradation of contaminants [23]. Since the inherent PFRs in ACFs initiate electron transfer in oxidative catalysis, they might be collaborated with the visible light-assisted photocatalysis to dramatically enhance the catalytic activity of Cit-Fe. Based on the above considerations, ACF was selected as the support to improve the catalytic activity of Cit-Fe in this study; peroxymonosulfate (PMS) were selected as the oxidant due to its outstanding characteristic. Compared to H_2O_2, PMS was easier to handle as it existed in the solid form. Furthermore, PMS could be activated to generate sulfate radicals ($SO_4^{\bullet-}$, 2.5–3.1 V vs NHE), which possess higher oxidizing capacity than $^{\bullet}OH$ (1.9–2.7 V, pH dependent), especially at higher pH levels [24–26]. Thus, we constructed a simple and practical catalytic oxidation system: FeCit@ACFs/PMS/visible light. It was used to bring about the decomposition of contaminants.

$$\mathrm{Fe(III)Cit} + h\nu \rightarrow \mathrm{Fe(II)} + \mathrm{Cit}^{\bullet 2-} \quad (1)$$

$$\mathrm{Fe(III)OHCit}^{-} + h\nu \rightarrow \mathrm{Fe(II)} + 3-\mathrm{HGA}^{\bullet 2-} \quad (2)$$

$$\mathrm{Fe(II)} + \mathrm{H_2O_2} \rightarrow \mathrm{Fe(III)} + {}^{\bullet}\mathrm{OH} + \mathrm{OH}^{-} \quad (3)$$

$$\mathrm{Fe(II)Cit}^{-} + \mathrm{H_2O_2} \rightarrow \mathrm{Fe(III)Cit} + {}^{\bullet}\mathrm{OH} + \mathrm{OH}^{-} \quad (4)$$

In this study, our aim is to investigate the catalytic activity of FeCit@ACFs and to comprehend the role of PFRs and visible light in a catalytic oxidation process. The decolorization of Reactive Red M-3BE (RR M-3BE) dye was selected as the model reaction to evaluate the catalytic oxidation performance of FeCit@ACFs/PMS/visible light system. Electron paramagnetic resonance (EPR) coupled with different scavengers (e.g., electron capture agents and radical scavengers) were used to investigate the mechanism through which PFRs exerted a positive effect on oxidative catalysis, and we also deciphered the synergistic effect of PFRs and visible light. In this study, we elucidated how PFRs could assist visible light-assisted photocatalytic degradation, offering a new insight into the positive role of PFRs. Thus, we presented a novel approach through which PFRs enhance the process of oxidative catalysis. Furthermore, we also paved the way towards developing robust processes that could be used for efficiently generating reactive oxidation species ROS ($SO_4^{\bullet-}$ and $^{\bullet}OH^{-}$): they are generally employed in environmental catalysis.

2. Experimental

2.1. Materials and reagents

Activated carbon fibers (ACFs) were bought from Jiangsu Sutong Carbon Fiber Co., Ltd. (Jiangsu, China). Ferric chloride hexahydrate ($FeCl_3{\cdot}6H_2O$), trisodium citrate dehydrate ($Na_3C_6H_5O_{7}{\cdot}H_2O$), PMS and hydrogen peroxide (30 wt%, Sinopharm Chemical Reagent Co. Ltd., Shanghai, China) were the analytical grade reagents used in this study. The spin trapping agent 5,5-dimethyl-pyrroline-*N*-oxide (DMPO) was supplied by Tokyo Chemical Industry Co. Ltd., Tokyo, Japan. Reactive Red M-3BE (RR M-3BE), Acid Red 1 (AR1), Rhodamine B (RHB), Acid Orange 7 (AO7), Methylene Blue (MB) and Basic Green 1 (BG1) were used as the model contaminants without further purification. The other chemical reagents used in this study were provided by Hangzhou Mike Chemical Instrument Co., Ltd. (Hangzhou, China). We used doubly distilled water throughout the experiment.

2.2. Catalyst preparation

Thirty grams of ACFs was impregnated with nitric acid solution (3 M), and the resulting suspension was maintained at 25 °C for 12 h. Then, the treated ACFs was taken out and rinsed repeatedly with distilled water. Finally, it was dried to obtain acidified ACFs. Ten grams of acidified ACFs was immersed in ferric citrate solution (2 mM, Fe (III): Cit = 1:1); the suspension was stored at 25 °C for 12 h. The treated ACFs was taken out from the solution and repeatedly rinsed with distilled water to remove free ferric citrate and other residues. Finally, it was dried at 60 °C to obtain the heterogeneous catalyst: FeCit@ACFs. On the heterogeneous catalyst FeCit@ACFs, we performed atomic absorption spectroscopy (Hitachi 170–70 atomic absorption spectrometer) and determined the iron content of FeCit@ACFs. From these measurements, we found that the ferric citrate ontent of FeCit@ACFs was 48.6 μmol g^{-1}.

2.3. Experimental procedures and analysis

In a magnetically stirred Pyrex reactor we carried out batch experiments to bring about the catalytic oxidation of the dyes. We used a 500 W mercury lamp as the source of light, while a 400 nm glass cut-off filter was used to exclude ultraviolet light. A 10-cm distance was maintained between the light source and reaction vessel. A constant temperature of 25 °C was maintained throughout the reaction. A reaction volume of 20 mL was used in all the experiments, and it contained the following initial concentrations: (a) dyes (50 μM, 20 mL); (b) supported catalyst FeCit@ACFs (2 g/L) or Cit-Fe (97.2 μM); and (c) oxidant PMS or H_2O_2. The values of apparent rate constant k_{obs} for the catalytic reaction can be obtained by determining the slope of the following plot: $\ln(C_t/C_0)$ versus time (see the Supporting information for details). At predetermined time intervals (3 min), samples were withdrawn from the flask and placed in an ultraviolet/visible (UV–vis) spectrophotometer (Hitachi U-3010) to determine the absorbance. Before adding the catalyst and oxidant, the pH of the initial solution was adjusted with NaOH or $HClO_4$.

Electron paramagnetic resonance (EPR) signals of ROS were trapped by DMPO and recorded at an ambient temperature in a Bruker A300 spectrometer (Bruker, Germany). The settings of EPR spectrometer were as follows: center field, 3520 G; sweep

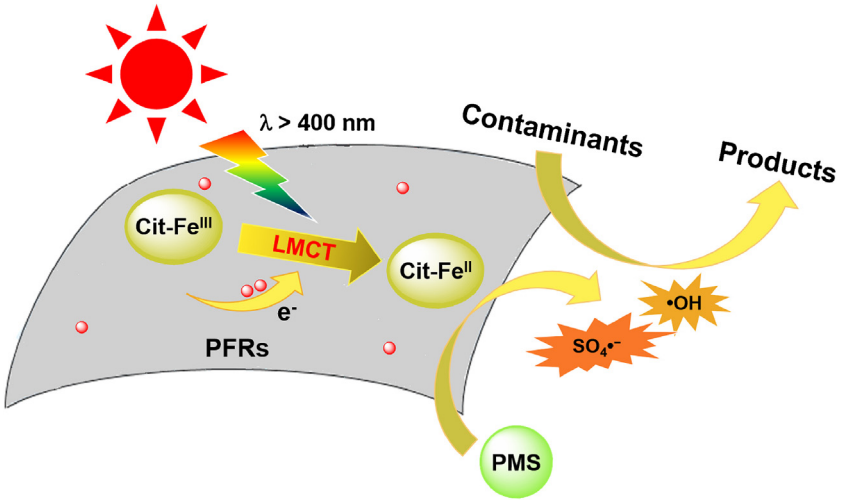

Scheme 1. The proposed catalytic oxidation mechanism in FeCit@ACFs/PMS/visible light system.

width, 100 G; microwave frequency, 9.77 GHz; modulation frequency, 100 kHz; and power, 12.72 mW. Furthermore, EPR signals of PFRs were recorded at 110 K using a Bruker A300 spectrometer. The settings of EPR spectrometer were as follows: center field, 3370 G; microwave frequency, 9.43 GHz; modulation frequency, 100 kHz; and power, 20.13 mW. Before performing the EPR test, we collected solid samples and dried them under vacuum. The binding site between ACFs and Fe ions was determined by performing X-ray photoelectron spectroscopy (XPS, Kratos Axis Ultra DLD, Kratos Analytical, Manchester, UK) under the following conditions: Al (mono) Kα irradiation ($h\nu$ = å1486.6 eV) was employed at pass energies of 160 eV (wide scan) and 20 eV (narrow scan). All the binding energy peaks of the XPS spectra were calibrated by considering the principal C1 s binding energy peak at 284.7 eV. The total number of electrons released during the oxidation process was detected by ABTS (2,2′-azino-bis (3-ethylbenzothiazoline-6-sulfonic acid)) method [27]. In order to determine the concentration of PMS in the system, we prepared samples by placing 1 mL of the reaction solution in a 4 mL cuvette. Then, 1 mL of 10 mM Fe(II) solution was acidified with 1 M H_2SO_4. Finally, 0.2 mL of a 0.3 M KSCN solution was added after 5 min. The absorbance was immediately recorded with a UV–vis spectrophotometer at a wavelength of 450 nm [28]. The concentration of H_2O_2 was measured by performing titanium potassium oxalate colorimetry [29].

3. Results and discussion

3.1. The catalytic oxidation activity

In this study, the catalytic oxidation performances of different systems were evaluated on the extent of removal of Reactive Red M-3BE (RR M-3BE), a hazardous dye as well as a common target contaminant for determining oxidizing capability. Fig. 1(A) showed the discoloration of RR M-3BE versus time under different systems. In Cit-Fe/PMS system (curve a), less than 18% of RR M-3BE dye was removed within 33 min. In FeCit@ACFs/PMS system (curve b), about 43% of RR M-3BE was removed, and the absorption performance of ACFs made inappreciable contributions to the removal of RR M-3BE (Fig. S1). The results indicated that the introduction of ACFs into Cit-Fe/PMS system significantly improved the oxidation efficiency of the system. Surprisingly, when FeCit@ACFs/PMS system was exposed to visible radiation (curve c), more than 97% of RR M-3BE was removed rapidly within 33 min: the characteristic absorption peak of RR M-3BE at 542 nm almost disappeared after the system underwent catalytic oxidation on being exposed to visible light (Fig. 1(B)). In addition, when the FeCit@ACFs/PMS system was exposed to visible light after keeping the reaction mixture in the dark for 12 min, the RR M-3BE removal also increased remarkably in the subsequent 21 min, with almost 89% of RR M-3BE being removed from the system. These results indicated that the introduction of visible light into FeCit@ACFs/PMS system sharply enhanced its oxidation efficiency.

To further investigate the effect of ACFs and visible light, we determined the variation of PMS concentration with time in different systems. As shown in Fig. 1(C), the consumption rates of PMS were determined as 12.7%, 23.5% and 36.3% for Cit-Fe/PMS, FeCit@ACFs/PMS and FeCit@ACFs/PMS/visible light system, respectively. To further understand the impact of ACFs and visible light on the system, we determined the oxidant utilization efficiency of PMS; this parameter was quantified by the oxidant consumption index (X): it is defined as the number of moles of oxidant consumed per mole of RR M-3BE removed. A lower value of X manifests a higher utilization efficiency of the oxidant [30]. As can be seen in the inset of Fig. 1(C), the FeCit@ACFs/PMS/visible light system (30.6) showed an extremely superior utilization efficiency of PMS as compared to those of Cit-Fe/PMS system (57.3) and FeCit@ACFs/PMS system without visible radiation (42.7). The aforementioned experimental results indicated that the introduction of ACFs and visible light enhanced the catalytic performance of Cit-Fe and thus significantly improved the utilization efficiency of PMS.

Given that reusability of a catalyst is a major concern in practical applications, we investigated the reusability performance of FeCit@ACFs system exposed to visible radiation. As can be seen in Fig. 1(D), the removal rate of RR M-3BE remained as high as 90% even after the fifth cycle. This indicated that the FeCit@ACFs retained stable catalytic activity and exhibited an excellent reusability performance, Therefore, FeCit@ACFs/visible light is a stable and environmentally friendly photocatalyst that can be used for activating PMS. Furthermore, we also investigated the pH adaptability of FeCit@ACFs/PMS/visible light system. Table S1 illustrates that the FeCit@ACFs/PMS/visible light system exhibits excellent pH adaptability, since the removal rate of RR M-3BE is more than 96% in the pH range of 2.0–11.0, which was significantly superior to the FeCit@ACFs/PMS system. Furthermore, we also determined the oxidation capacity of FeCit@ACFs/PMS/visible light system by determining the extent of removal of other organic dyes including Acid Red 1 (AR1), Rhodamine B (RHB), Acid Orange 7 (AO7), Methylene Blue (MB) and Basic Green 1 (BG1). The results are

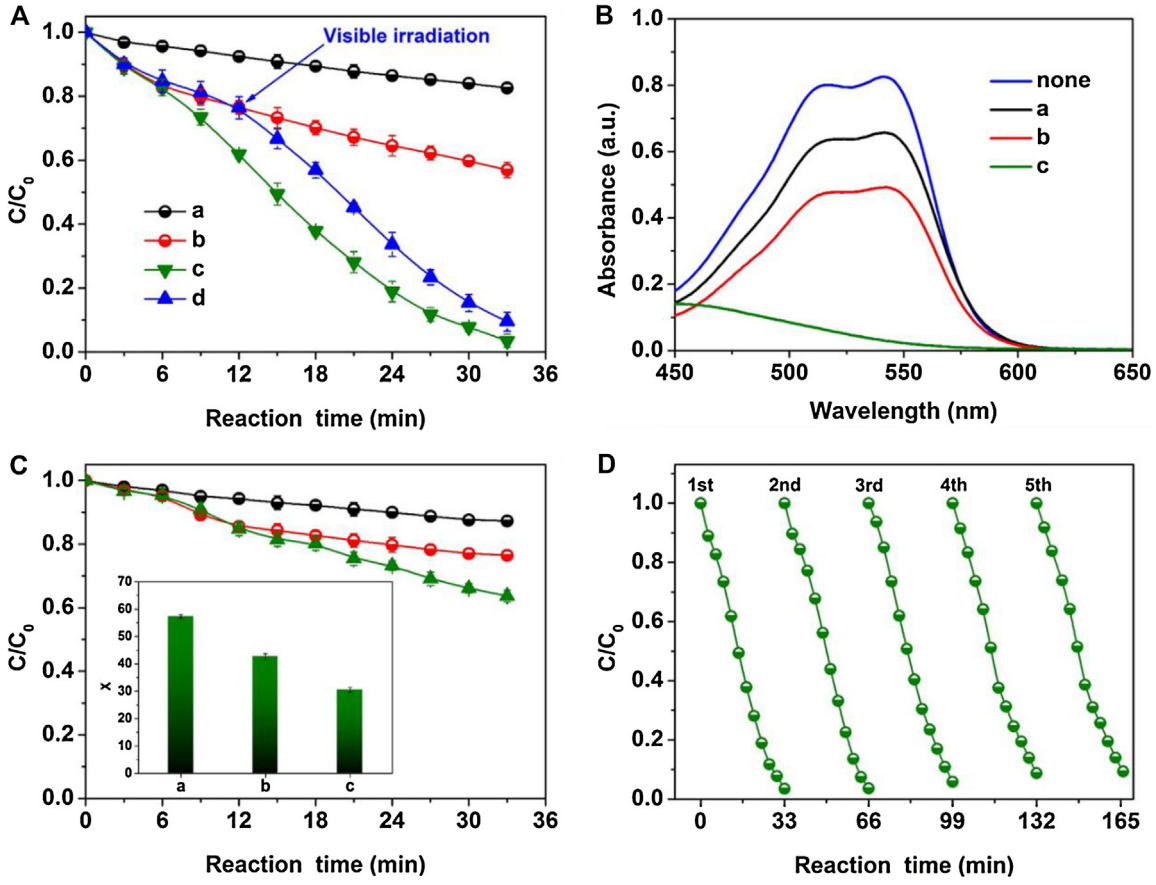

Fig. 1. (A) Time profiles of RR M-3BE decolorization in different systems: (a) Cit-Fe/PMS; (b) FeCit@ACFs/PMS (in the dark); (c) FeCit@ACFs/PMS/visible light; (d) after keeping the reaction mixture in dark for 12 min, the samples are exposed to visible light. (B) UV–vis spectra depicting the removal of RR M-3BE by different systems within 33 min. (C) The variation of PMS concentration with reaction time in different systems, and the inset showed the utilization efficiency of PMS in corresponding systems. (D) Repeated recycling of FeCit@ACFs with PMS for the removal of RR M-3BE. Reaction conditions: [FeCit@ACFs] = 2 g/L, [Cit-Fe] = 97.2 μM, [PMS] = 4 mM, [RR M-3BE] = 50 μM, initial pH 10.0, T = 25 °C.

presented in Table S2. Based on the results, we have the following inference: when FeCit@ACFs/PMS system is exposed to visible light, the removal of other representative dyes, such as acid dyes, fluorescent dyes, and basic dyes is significantly enhanced; this finding can be effectively applied to environmental remediation.

3.2. Analysis of catalytic oxidation mechanism

In the oxidation process based on PMS, the oxidation of organic contaminants was primarily triggered by ROS. Therefore, butanol (TBA) and methanol (MA) were used to investigate the involved ROS in FeCit@ACFs/PMS/visible light system; their rate constants were different for reactions with sulfate radicals ($SO_4^{\bullet-}$) and hydroxyl radicals ($^{\bullet}OH$). MA showed high reactivity with both the species ($k_{^{\bullet}OH/MA} = 9.7 \times 10^8\ M^{-1}\ s^{-1}$, $k_{SO4^{\bullet-}/MA} = 1.6 \times 10^7\ M^{-1}\ s^{-1}$), while TBA exhibited high reactivity with $^{\bullet}OH$ ($k_{^{\bullet}OH/TBA} = (3.8–7.6) \times 10^8\ M^{-1}\ s^{-1}$) and a relatively low reactivity with $SO_4^{\bullet-}$ ($k_{SO4^{\bullet-}/TBA} = (4.0–9.1) \times 10^5\ M^{-1}\ s^{-1}$) [31–33]. As can be seen in Fig. 2(A), when excess TBA (1 M) was added into FeCit@ACFs/PMS/visible light system, the removal rate of RR M-3BE decreased sharply from 97.5% to 46.1%; k_{obs} also decreased from 0.09555 min^{-1} to 0.01781 min^{-1}. This indicates that $^{\bullet}OH$ was generated and it played an important role in the oxidation process. Furthermore, when excess MA (1 M) was added, the inhibitory effect of MA on RR M-3BE removal was more obvious than that of TBA, because the removal rate further decreased to 24.4%; k_{obs} also decreased to 0.00716 min^{-1}. This indicates that $SO_4^{\bullet-}$ was also generated in FeCit@ACFs/PMS/visible light system.

To further reveal the role of $^{\bullet}OH$ and $SO_4^{\bullet-}$, EPR spin-trap experiments were performed using DMPO as the trapping reagent. As shown in Fig. 2(B), a four-line signal and a six-line signal, the characteristic spectra of adducts DMPO–$^{\bullet}OH$ and DMPO–$SO_4^{\bullet-}$, were observed in FeCit@ACFs/PMS/visible light system, indicating that $^{\bullet}OH$ and $SO_4^{\bullet-}$ were involved in the oxidation reaction. This observation is in good agreement with the phenomena shown in Fig. 2(A). Furthermore, the intensity of the DMPO–$^{\bullet}OH$ and DMPO–$SO_4^{\bullet-}$ signals were much stronger in FeCit@ACFs/PMS/visible light system than that in Cit-Fe/PMS and FeCit@ACFs/PMS systems, indicating that a greater number of $^{\bullet}OH$ and $SO_4^{\bullet-}$ radicals were generated in FeCit@ACFs/PMS/visible light system. All these observations suggest that the introduction of ACFs and visible light promoted the generation of $^{\bullet}OH$ and $SO_4^{\bullet-}$ radicals, which subsequently enhanced the oxidation efficiency of the system.

In general, the electrons released during oxidation reactions play a pivotal role in the generation of $^{\bullet}OH$ and $SO_4^{\bullet-}$ radicals [34]. Therefore, it is essential to investigate the electron transfer process in FeCit@ACFs/PMS/visible light system. Herein, the ABTS was used to determine the amount of electrons released during the oxidation reaction [27]. As shown in Fig. 2(C), the number of detected electrons in FeCit@ACFs/PMS system was greater than that in Cit-Fe/PMS system. This indicates that the electron transfer process was accelerated with the introduction of ACFs. Considering PFRs in ACFs might impact the electron transfer behavior during the oxidation process, we used the EPR technique to investigate the PFRs change in ACFs. As can be seen in Fig. 2(D), the signal intensity of PFRs in ACFs decreased sharply after the reaction, indicating

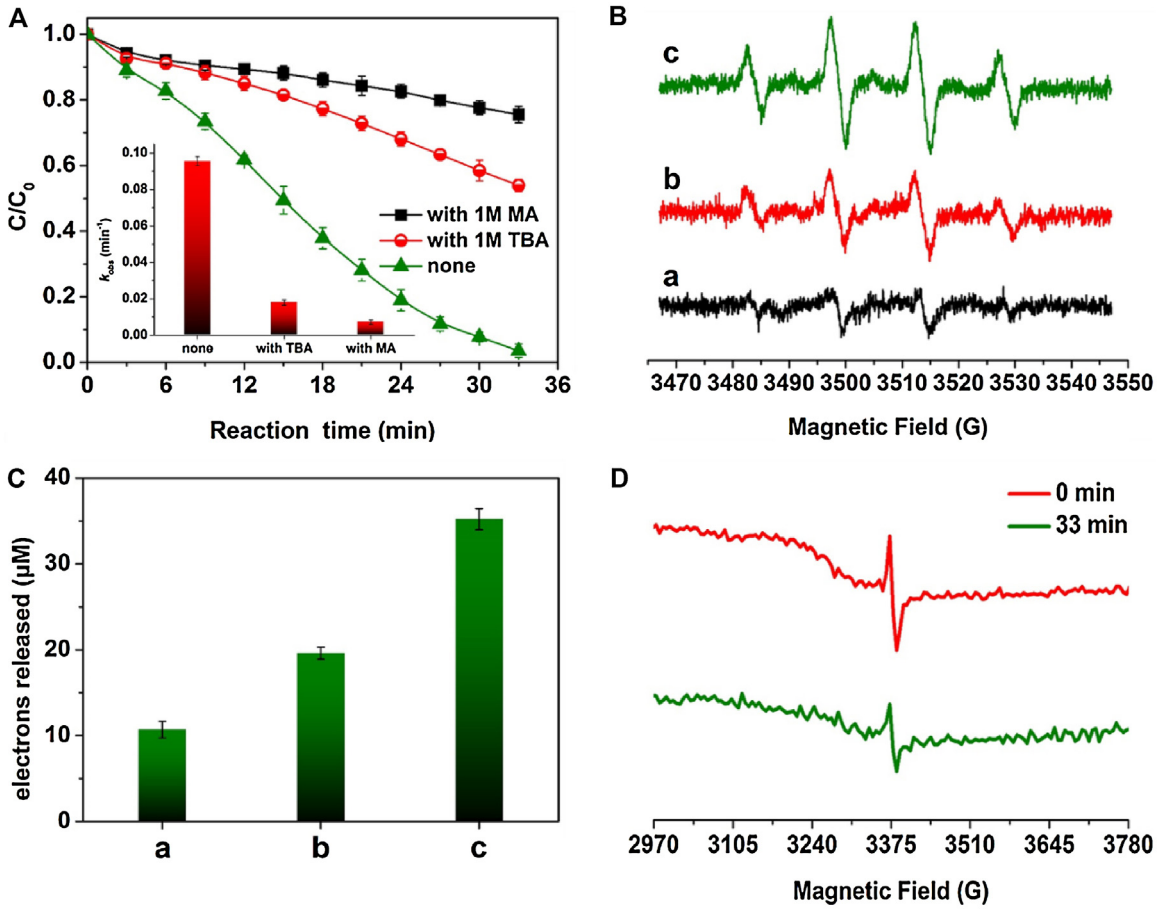

Fig. 2. (A) Effects of tertiary butanol (TBA) and methanol (MA) on the removal of RR M-3BE in FeCit@ACFs/PMS/visible light system; the inset shows k_{obs} of corresponding systems. (B) DMPO spin-trapping EPR spectra in different systems: (a) Cit-Fe/PMS; (b) FeCit@ACFs/PMS (in the dark); (c) FeCit@ACFs/PMS/visible light. (C) Electrons released during oxidation reactions in different systems. (D) EPR spectra of FeCit@ACFs at 110 K at different reaction times in FeCit@ACFs/PMS/visible light systems. Reaction conditions: [FeCit@ACFs] = 2 g/L, [PMS] = 4 mM, [RR M-3BE] = 50 μM, initial pH 10.0, T = 25 °C.

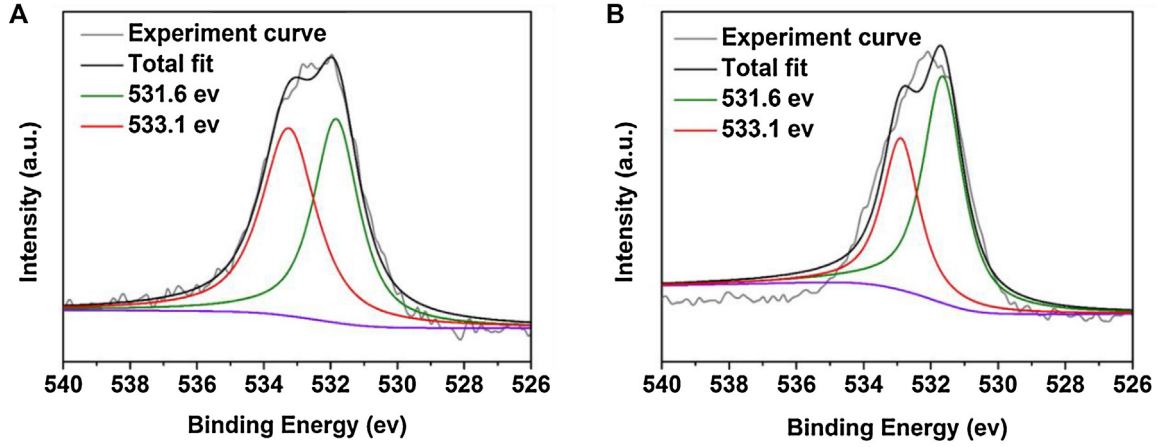

Fig. 3. XPS spectra of O 1 s in (A) fresh FeCit@ACFs and (B) FeCit@ACFs after its utilization in the FeCit@ACFs/PMS/visible light system.

that PFRs in ACFs might be responsible for the electron transfer during the oxidation process. To further get deep insight into the electron-donating behavior of ACFs in FeCit@ACFs/PMS/visible light system, we conducted X-ray photoelectron spectroscopy and determined the change in the structure of FeCit@ACFs after the reaction. As shown in Fig. 3(A), for the fresh FeCit@ACFs, the O 1s peaks appeared at 531.6 eV and at 533.1 eV: these peaks were assigned to oxygen atom in the carbonyl group (C═O) and the oxygen atom in the hydroxyl group (—O—H), respectively [35]. However, after the reaction, there was a decrease in the intensity of the peak representing oxygen in —O—H group; on the other hand, there was an increase in the intensity of the peak ascribed to oxygen in C═O bond (Fig. 3(B)), This indicates that during the reaction, there was conversion of C—O—H to C═O; the conversion was ascribed to the electron transfer from PFRs in ACFs to Cit-Fe, leading to the transformation from Cit-Fe^{III} to Cit-Fe^{II} species [35]. In addition,

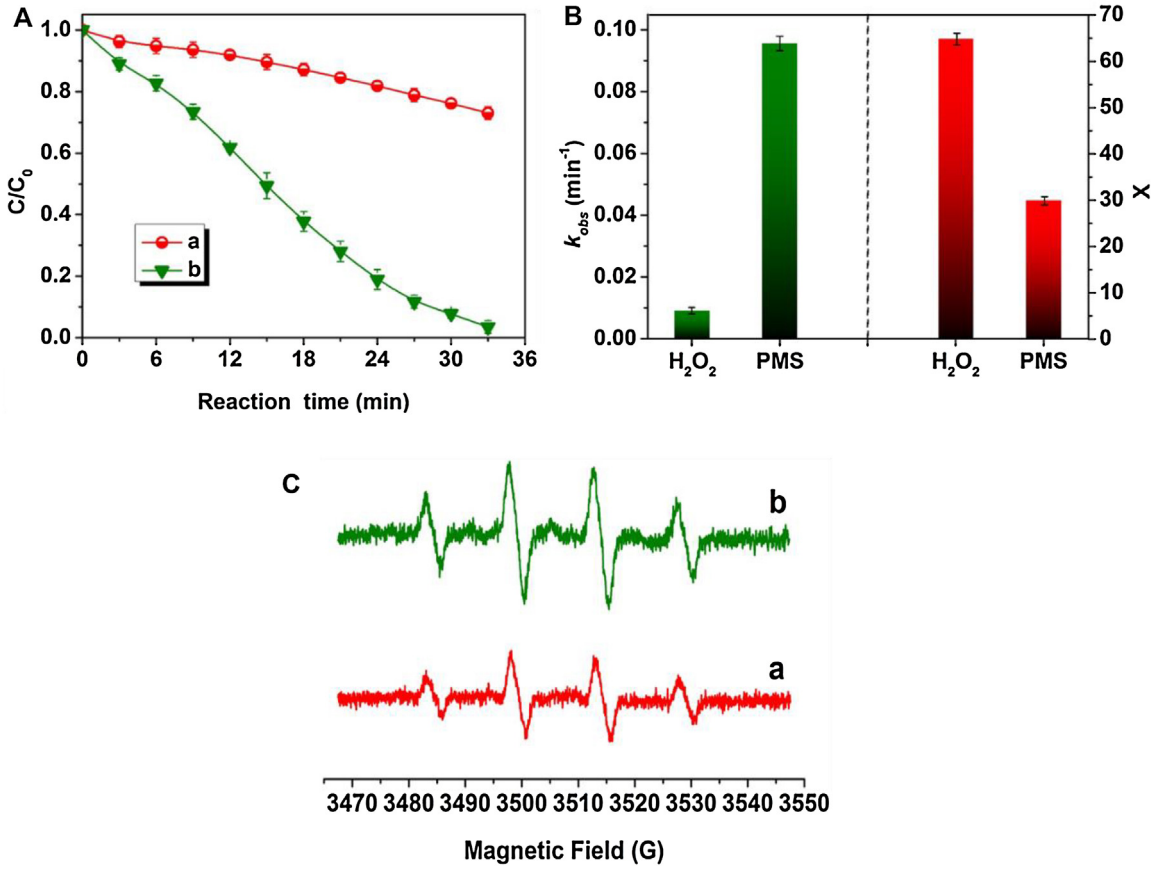

Fig. 4. (A) Time profiles of RR M-3BE decolorization in FeCit@ACFs/H_2O_2/visible light system (curve a) and FeCit@ACFs/PMS/visible light system (curve b). (B) A comparison of rate constants of apparent pseudo-first-order rate constants and the oxidant consumption indices of FeCit@ACFs/H_2O_2/visible light system and FeCit@ACFs/PMS/visible light system. (C) DMPO spin-trapping EPR spectra in FeCit@ACFs/H_2O_2/visible light system (curve a) and FeCit@ACFs/PMS/visible light system (curve b). Reaction conditions: [FeCit@ACFs] = 2 g/L, [PMS] = [H_2O_2] = 4 mM, [RR M-3BE] = 50 μM, initial pH 10.0, T = 25 °C.

it is worth noting that the electron transfer of FeCit@ACFs/PMS system was further enhanced when exposed to visible radiation (Fig. 2(C)), which could be attribute to the high intrinsic photosensitivity of Cit-Fe. Cit-Fe complexes have been proved to be outstanding Fe(III)–photocatalysts with high photoreactivity, and Paweł et al. have reported that when Cit-Fe/H_2O_2 system was irradiated with sunlight, the LMCT pathways were stimulated; these pathways accelerated the catalytic activity of Cit-Fe complexes, thereby increasing the generation of •OH radicals [17].

Based on the above results and analysis, we proposed a possible reaction mechanism (Scheme 1). First, PFRs in ACFs act as an electron sink and donate electrons to Cit-Fe complexes, which accelerated the LMCT processes. Meanwhile, visible radiation can serve as another powerful assistor to further enhance the LMCT processes since Cit-Fe complexes have highly intrinsic photosensitivity. The synergistic effect of PFRs and visible light enhanced the reaction rate-determining step of the reduction reaction involving the conversion of Cit-Fe^{III} to Cit-Fe^{II} species; these species play a key role in improving the catalytic activity of the constructed FeCit@ACFs catalyst. Thus, in the presence of visible light, FeCit@ACFs acts as a strong catalyst and effectively activates PMS to generate •OH and $SO_4^{\bullet-}$ radicals, which play an important role in the decomposition of contaminants

3.3. Comparison of FeCit@ACFs/PMS/visible light system and FeCit@ACFs/H_2O_2/visible light system

Based on the above experimental results, we concluded that the introduction of ACFs and visible light into Cit-Fe/PMS system dramatically improve the catalytic activity of Cit-Fe, thereby increasing the oxidation efficiency and increased the utilization efficiencies of PMS. In order to further assess the oxidation performance of FeCit@ACFs/PMS/visible light system, we performed test experiments using hydrogen peroxide (H_2O_2), one of the most commonly oxidants for the treatment of contaminants, was also employed in test experiments [36–38]. As shown in Fig. 4(A), only 27.0% of RR M-3BE was removed in 33 min in FeCit@ACFs/H_2O_2/visible light system (curve a), indicating that the oxidizing efficiency of this system was far inferior to that of FeCit@ACFs/PMS/visible light system (curve b). To further assess the difference in catalytic oxidation activity of these two systems, we adopted a general pseudo-first order kinetic model ($\ln(C_t/C_0)/k_{obs}t$). As shown in Fig. 4(B), k_{obs} for FeCit@ACFs/PMS/visible light system was calculated to be 0.09555 min^{-1}, which was 10.5-fold higher than that for FeCit@ACFs/H_2O_2/visible light system (0.00909 min^{-1}). Furthermore, we also compared the efficiency of oxidant utilization in the PMS and H_2O_2 systems. As can be seen in Fig. 4(B), the efficiency of oxidant utilization in FeCit@ACFs/PMS/visible light system was determined to be 30.2; this value of utilization efficiency was dramatically superior to that of FeCit@ACFs/H_2O_2/visible light system (66.3). In summary, the experimental results indicate that the catalytic oxidation performance by FeCit@ACFs/PMS/visible light system is much more superior to that of FeCit@ACFs/H_2O_2/visible light system.

In addition, the generated ROS of the two systems were also compared. As shown in Fig. 4(C), a typical four-peak spectrum of DMPO–•OH was observed in the two systems and the intensity of the DMPO–•OH signal in FeCit@ACFs/PMS/visible light system

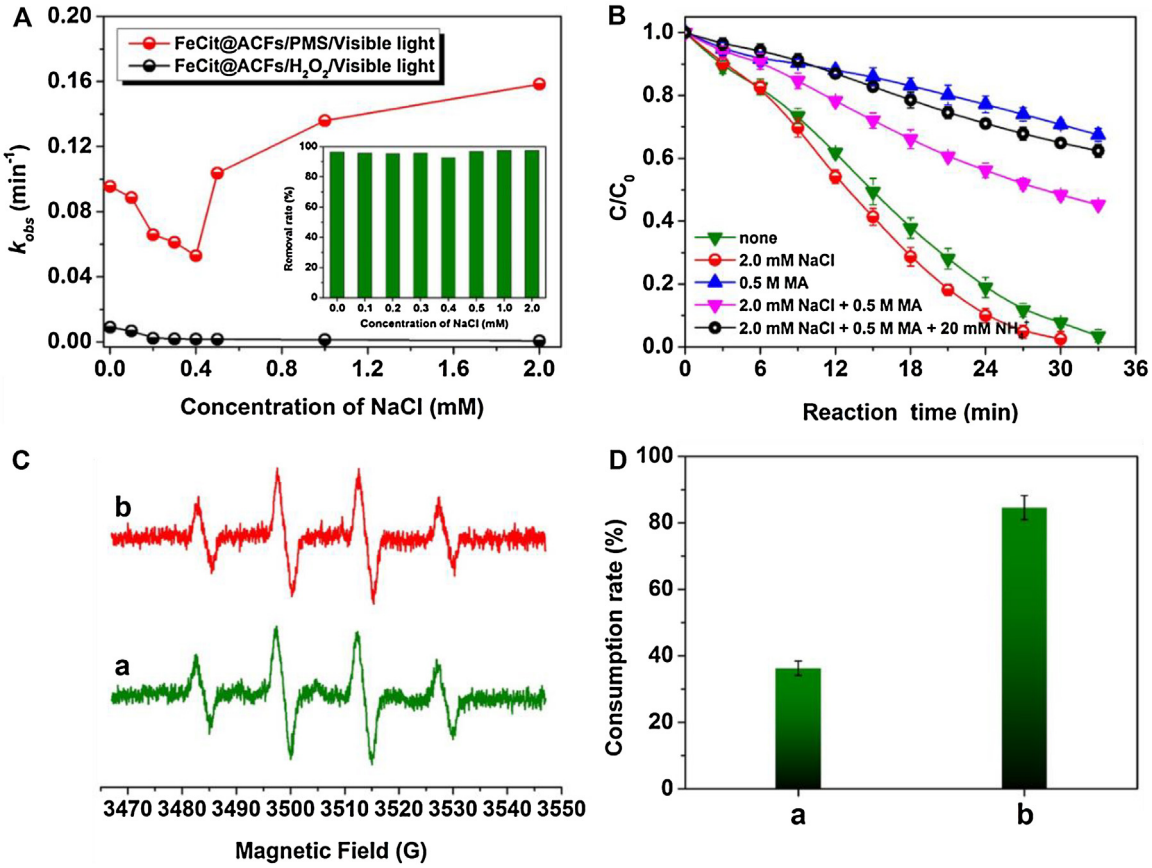

Fig. 5. (A) The variation in k_{obs} values with increasing NaCl concentrations in different systems, and the inset showed how the removal rate of RR M-3BE in FeCit@ACFs/PMS/visible light system varied with the addition of different concentrations of NaCl. (B) Time profiles of RR M-3BE decolorization in FeCit@ACFs/PMS/visible light system with the addition of different reagents. (C) DMPO spin-trapping EPR spectra in the following systems: (a) FeCit@ACFs/PMS/visible light system and (b) FeCit@ACFs/PMS/visible light system with the addition of 2.0 mM NaCl. (D) The consumption rate of PMS in the following systems: (a) FeCit@ACFs/PMS/visible light system and (b) FeCit@ACFs/PMS/visible light system with the addition of 2.0 mM NaCl. Reaction conditions: [FeCit@ACFs] = 2 g/L, [PMS] = 4 mM, [RR M-3BE] = 50 μM, initial pH 10.0, T = 25 °C. (For interpretation of the references to color in the text, the reader is referred to the web version of this article.)

was much stronger, suggesting that FeCit@ACFs/PMS/visible light system generate a higher concentration of •OH. In addition, the characteristic spectra of DMPO–SO_4•$^-$ adducts was only observed in FeCit@ACFs/PMS/visible light system, demonstrating that extra SO_4•$^-$ was generated in this system. The higher concentration of •OH and extra SO_4•$^-$ was responsible for the more excellent catalytic oxidation performance of FeCit@ACFs/PMS/visible light.

Sodium chloride (NaCl), one of the most abundant ions in practical water, is used widely in the textile printing and dyeing industry to accelerate the dyes transfer from the aqueous phase to the fiber phase. Therefore, it is indispensable to research the influence of NaCl on the oxidative activity of the two systems. As shown in Fig. 5(A), there was a decrease in k_{obs} value of RR M-3BE removal in FeCit@ACFs/H_2O_2/visible light system when the concentration of NaCl was increased from 0 to 2.0 mM. This variation in k_{obs} values could be attributed to the hydroxyl radical scavenging effects of NaCl. In FeCit@ACFs/PMS/visible light system, the k_{obs} value decreased steadily as the NaCl concentrations were increased from 0 to 0.4 mM. However, when NaCl concentration exceeded 0.4 mM, the k_{obs} values increased with a further increase in NaCl concentration. Moreover, the removal rates of RR M-3BE remained consistently high at 93%, with a steady increase in the concentrations of NaCl (the inset of Fig. 5(A)). This indicates that the addition of high concentration of NaCl had a positive effect on the removal of RR M-3BE in FeCit@ACFs/PMS/visible light system; this observation contradicted previous reports stating that at higher concentrations, NaCl could capture radical species and thus dramatically hamper the treatment of dyestuff wastewater by common AOPs [39]. It is an additional advantage for the practical application of the FeCit@ACFs/PMS/visible light system.

To get a deep insight into underlying mechanism through which the oxidation performance of FeCit@ACFs/PMS/visible light system is enhanced in the presence of high NaCl concentration, we used methanol (MA) to detect the variation of ROS. Note that MA is a trapping agent for both •OH and SO_4•$^-$ radicals. As shown in Fig. 5(B), the removal of RR M-3BE was enhanced with the addition of 2.0 mM NaCl (red line). When excessive MA (0.5 M) was added into FeCit@ACFs/PMS/visible light/NaCl (2.0 mM) system, the removal of RR M-3BE weakened dramatically (pink line), but still remarkably superior to the removal efficiency of FeCit@ACFs/PMS/visible light/MA system (blue line), which was devoid of NaCl. The results indicate that a high concentrations of NaCl may be either enhancing the generation of •OH and SO_4•$^-$ or promoting the generation of other types of ROS. Therefore, we performed EPR to detect the concentrations of •OH and SO_4•$^-$ in FeCit@ACFs/PMS/visible light/NaCl (2.0 mM) system. As can be seen in Fig. 5(C), there was a negligible change in the peak intensities of adducts DMPO-•OH and DMPO-SO_4•$^-$ adducts in FeCit@ACFs/PMS/visible light system with the addition of NaCl, indicating that the addition of high concentration of NaCl could not enhance the generation of •OH and SO_4•$^-$. However, the consumption rate of PMS increased dramatically with the addition of NaCl (Fig. 5(D)). Therefore, we speculated that a high concentration of Cl^- directly reacted with PMS to generate hypochlorous acid (HOCl), which success-

fully removed the organic pollutant through its strong oxidizing effect (Reaction (5)), and thus positively impacted the oxidation performance of the system [40,41]. In order to verify our speculation, we included the scavenger radical NH_4^+ as it readily reacts with HOCl, but it cannot be easily oxidized by •OH and $SO_4^{\bullet-}$. Fig. 5(B) illustrates that when NH_4^+ was further added into FeCit@ACFs/PMS/visible light/MA/NaCl (2.0 mM) system (•OH and $SO_4^{\bullet-}$ has been completely scavenged by MA in this system.), the RR M-3BE removal was further retarded; moreover, the removal process (green line) was almost coincided with the removal process in FeCit@ACFs/PMS/visible light/MA system (blue line), suggesting that the decoloration process was completely inhibited by the further addition of NH_4^+. The results were in agreement with our conjecture that HOCl is generated in FeCit@ACFs/PMS/visible light system when a high concentration of NaCl is added.

$$HSO_{5^-} + Cl^- \rightarrow SO_4{}^{2-} + HOCl \quad (5)$$

4. Conclusion

In this study, the PFRs of ACFs were integrated with Fe(III)–photocatalysts to construct a novel and highly efficient catalytic oxidation system: FeCit@ACFs/PMS/visible lights. The system possessed an outstanding adaptability in the pH range of 2–11. Furthermore, it also exhibited an excellent catalytic oxidation performance: the reactions rates of RR M-3BE removal were increased by about 6.1 times and 17.1 times compared to those involving the sole use of FeCit@ACFs/PMS system and Cit-Fe/PMS system, respectively. Moreover, FeCit@ACFs/PMS/visible lights system exhibited greater oxidation capacity and higher efficiency of oxidant utilization compared to the previously reported FeCit@ACFs/H_2O_2/visible lights system. By investigating the reaction mechanism, we found that PFRs in ACFs served as an electron sink and provided electrons to Cit-Fe, thereby accelerating the LMCT processes that govern the rate-determining step of the reduction reaction that transforms Cit-Fe^{III} into Cit-Fe^{II}. Moreover, visible radiation further enhances the LMCT processes since Cit-Fe exhibits high photosensitivity. Owing to the synergistic effect of PFRs and visible light, the transformation from Fe(III) to Fe(II) was dramatically accelerated. Consequently, the generation of highly reactive •OH and $SO_4^{\bullet-}$ species was also enhanced. The findings of this study offer a new insight into the positive role of PFRs and present a promising research domain of PFRs-enhanced catalytic performance. In addition, they paved the way toward developing robust processes for the generation of highly active ROS, which could be employed in environmental catalysis.

Acknowledgments

This work was supported by the State Key Program of National Natural Science of China (No. 51133006), the National Natural Science Foundation of China (No. 51302246), the Public Welfare Technology Application Research Project of Zhejiang Province (No. 2016C31076) and Zhejiang Provincial Natural Science Foundation of China (No. LY14E030015, LQ15E030005).

Appendix A. Supplementary data

Supplementary data associated with this article can be found, in the online version, at http://dx.doi.org/10.1016/j.apcatb.2016.12.060.

References

[1] E. Vejerano, S.M. Lomnicki, B. Dellinger, Environ. Sci. Technol. 46 (2012) 9406–9411.
[2] S. Lomnicki, H. Truong, E. Vejerano, B. Dellinger, Environ. Sci. Technol. 42 (2008) 4982–4998.
[3] A.L.N. Dela Cruz, W. Gehling, S. Lomnicki, R. Cook, B. Dellinger, Environ. Sci. Technol. 45 (2011) 6356–6365.
[4] A.L.N. Dela Cruz, R.L. Cook, S.M. Lomnicki, B. Dellinger, Environ. Sci. Technol. 46 (2012) 5971–5978.
[5] S. Balakrishna, S. Lomnicki, K.M. McAvey, R.B. Cole, B. Dellinger, S.A. Cormier, Part. Fibre Toxicol. 6 (2009) 11.
[6] P.T. Thevenot, J. Saravia, N.L. Jin, J.D. Giaimo, R.E. Chustz, S. Mahne, M.A. Kelley, V.Y. Hebert, B. Dellinger, T.R. Dugas, F.J. DeMayo, S.A. Cormier, Am. J. Respir. Cell Mol. 48 (2013) 189–197.
[7] S. Balakrishna, J. Saravia, P. Thevenot, T. Ahlert, S. Lominiki, B. Dellinger, S.A. Cormier, Part. Fibre Toxicol. 8 (2011) 11.
[8] G.D. Fang, J. Gao, C. Liu, D.D. Dionysiou, Y. Wang, D.M. Zhou, Environ. Sci. Technol. 48 (2014) 1902–1910.
[9] G.D. Fang, C. Liu, J. Gao, D.D. Dionysiou, D.M. Zhou, Environ. Sci. Technol. 49 (2015) 5645–5653.
[10] L. Khachatryan, E. Vejerano, S. Lomnicki, B. Dellinger, Environ. Sci. Technol. 45 (2011) 8559–8566.
[11] L. Khachatryan, B. Dellinger, Environ. Sci. Technol. 45 (2011) 9232–9239.
[12] L.F. Yin, Z.Y. Shen, J.F. Niu, J. Chen, Y.P. Duan, Environ. Sci. Technol. 44 (2010) 9117–9122.
[13] C. Cai, Z.Y. Zhang, J. Liu, N. Shan, H. Zhang, D.D. Dionysiou, Appl. Catal. B: Environ. 182 (2016) 456–468.
[14] C.C. Chen, W.H. Ma, J.C. Zhao, Chem. Soc. Rev. 39 (2010) 4206–4219.
[15] Y. Chen, Z.Z. Liu, Z.P. Wang, M.M. Xue, X.C. Zhu, T. Tao, J. Hazard. Mater. 194 (2011) 202–208.
[16] M.R.A. Silva, A.G. Trovó, R.F.P. Nogueira, J. Photochem. Photobiol. A 191 (2007) 187–192.
[17] P. Ciesla, P. Kocot, P. Mytych, Z. Stasicka, J. Mol. Catal. A-Chem. 224 (2004) 17–33.
[18] S. Parra, L. Henao, E. Mielczarski, J. Mielczarski, P. Albers, E. Suvorova, J. Guindet, J. Kiwi, Langmuir 20 (2004) 5621–5629.
[19] R.G. Olmos, M.J. Martin, A. Georgi, F.D. Kopinke, I. Oller, S. Malato, Appl. Catal. B: Environ. 125 (2012) 51–58.
[20] H.W. Ji, W.J. Song, C.C. Chen, H. Yuan, W.H. Ma, J.C. Zhao, Environ. Sci. Technol. 41 (2007) 5103–5107.
[21] M.M. Cheng, W.H. Ma, C.C. Chen, J.N. Yao, J.C. Zhao, Appl. Catal. B: Environ. 65 (2006) 217–226.
[22] Z.F. Huang, H.W. Bao, Y.Y. Yao, W.Y. Lu, W.X. Chen, Appl. Catal. B: Environ. 154–155 (2014) 36–43.
[23] Y.Y. Yao, B. Jiang, Y.J. Mao, J. Chen, Z.F. Huang, S.Q. Huang, L. Zhang, Chem. Commun. 51 (2015) 16139–16142.
[24] S.L. Luo, L. Duan, B.Z. Sun, M.Y. Wei, X.X. Li, A.H. Xu, Appl. Catal. B: Environ. 164 (2015) 92–99.
[25] G.P. Anipsitakis, D.D. Dionysiou, Environ. Sci. Technol. 37 (2003) 4790–4797.
[26] Y.J. Yao, Y.M. Cai, G.D. Wu, F.Y. Wei, X.Y. Li, H. Chen, S.B. Wang, J. Hazard. Mater. 296 (2015) 128–137.
[27] S.E. Page, G.W. Kling, M. Sander, K.H. Harrold, J.R. Logan, K. McNeill, R.M. Cory, Environ. Sci. Technol. 47 (2013) 12860–12867.
[28] Z.H. Wang, R.T. Bush, L.A. Sullivan, C.C. Chen, J.S. Liu, Environ. Sci. Technol. 48 (2014) 3978–3985.
[29] G.M. Eisenberg, Ind. Eng. Chem. Anal. Ed. 15 (1943) 327–328.
[30] R.G. Olmos, F.D. Kopinke, K. Mackenzie, A. Georgi, Environ. Sci. Technol. 47 (2013) 2353–2360.
[31] P. Wang, S.Y. Yang, L. Shan, R. Niu, X.T. Shao, J. Environ. Sci. 23 (2011) 1799–1807.
[32] G.P. Anipsitakis, D.D. Dionysiou, Environ. Sci. Technol. 38 (2004) 3705–3712.
[33] F. Gong, L. Wang, D.W. Li, F.Y. Zhou, Y.Y. Yao, W.Y. Lu, S.Q. Huang, W.X. Chen, Chem. Eng. J. 267 (2015) 102–110.
[34] S.E. Page, M. Sander, W.A. Arnold, K. McNeill, Environ. Sci. Technol. 46 (2012) 1590–1597.
[35] F. Gong, L.S. Luo, Y.Y. Yao, D.J. Dai, W.Y. Lu, W.X. Chen, Chem. Eng. J. 304 (2016) 440–447.
[36] Y. Li, B. Wen, W.H. Ma, C.C. Chen, J.C. Zhao, Environ. Sci. Technol. 46 (2012) 5093–5099.
[37] L.S. Luo, Y.Y. Yao, F. Gong, Z.F. Huang, W.Y. Lu, W.X. Chen, L. Zhang, RSC Adv. 6 (2016) 47661–47668.
[38] O.A. Makhotkina, S.V. Preis, E.V. Parkhomchuk, Appl. Catal. B: Environ. 84 (2008) 821–826.
[39] R.X. Yuan, S.N. Ramjaun, Z.H. Wang, J.S. Liu, Chem. Eng. J. 192 (2012) 171–178.
[40] G.P. Anipsitakis, T.P. Tufano, D.D. Dionysiou, Water. Res. 42 (2008) 2899–2910.
[41] G.P. Anipsitakis, D.D. Dionysiou, M.A. Gonzalez, Environ. Sci. Technol. 40 (2006) 1000–1007.